J Bio Tribo Corros (2017) 3:41
DOI 10.1007/s40735-017-0096-x

Effect of Acid Treatment on the Surface Modification of Ti-6Al-7Nb and Ti-5Al-2Nb-1Ta and Its Electrochemical Investigations in Simulated Body Fluid

Y. Sasikumar[1] · N. Rajendran[1]

Received: 20 March 2017 / Revised: 19 June 2017 / Accepted: 20 June 2017 / Published online: 19 July 2017

Abstract Ti-6Al-7Nb and Ti-5Al-2Nb-1Ta specimens were subjected to two-step chemical treatments by mixture of acids ($HCl + H_2SO_4$) followed by alkali (NaOH) and heat treatment to produce a porous anatase gel layer which enhances the osseointegration. The influence of immersion time on the behaviour of the treated alloys in SBF was investigated using X-ray diffraction and scanning electron microscopy analyses and Fourier transform infrared spectroscopy analysis. Polarization study exhibited that the specimens after immersion in SBF solution showed high corrosion resistance which is attributed to the apatite growth on surface-modified Ti-6Al-7Nb and Ti-5Al-2Nb-1Ta surfaces.

Keywords Acid treatment · Titanium alloys · In vitro bioactivity · Apatite · Porous layer

1 Introduction

Titanium and its alloys are used in biomedical applications owing to their favourable mechanical properties, good biocompatibility and excellent corrosion resistance [1, 2]. Ti-6Al-4V alloy with ($\alpha + \beta$) structure was used as a conventional implant material for orthopaedic implants. It was found that the vanadium (V) present in the alloy could be released into the cell tissue due to the dissolution and wear process [3–5]. Moreover, V is classified in the toxic group [6]. Hence, it becomes necessary to select non-toxic alloying elements for biomedical applications. Vanadium-free Ti alloys like Ti-6Al-7Nb and Ti-5Al-2Nb-1Ta are being used as an alternative to Ti-6Al-4V, where V is replaced by Nb and Ta which is also a β-phase stabilizer. Research studies revealed that Ta, Nb, Zr and Mo are non-toxic and also these elements could enhance the long-term biocompatibility [7–9]. Besides, they are expected to improve the mechanical properties and corrosion resistance as well.

Titanium alloy is the most commonly preferred metallic biomaterials. When the metallic implant is placed inside the living system, the electrochemical reaction degrades the metal surface called corrosion, due to the presence of corrosive environment that includes water, sodium, chlorine, proteins, plasma and amino acids [10, 11]. The major problems related to metallic biomaterials are the compatibility with the blood and corrosion of metallic materials which are the main cause of rejection of metallic implants [12].

To tackle the above-mentioned limitations, a number of strategies were implemented to change the surface for the compatibility and corrosion resistance enhancement of the biomaterial known as surface modification [13]. The surface of the material has an important part in the response of biological system towards implant. After implantation, the communications between the implant surface and the biological system will not be affected, which means that the body should not treat the biomaterial as an external thing that will be achieved through effective selection of a material with desired properties. The required characteristics different from the naive material of the implant surface are attained through surface modification [14].

Ti-based alloys are basically subjected to surface modification to enhance the resistivity towards corrosion, osseointegration also the biocompatibility for its applications in the medical field. The factors affecting the

✉ N. Rajendran
nrajendran@annauniv.edu

[1] Department of Chemistry, Anna University, Chennai 600 025, India

osseointegration of metallic implants are the mechanical properties and the interaction of a metal surface with the biological system. If the body treats the metal implant as a foreign substance, the adherence of platelets activates the coagulation cascade which results in metal corrosion associated with inflammation. The corroded particles of the metallic implant may engulf by the macrophages or the implant weakens. The implant rejection can be reduced by improving the surface properties through the surface modification techniques. Hence, surface treatments of Ti and Ti-based alloy implants are required to enhance osseointegration, improve tissue adhesion and decrease bacterial adhesion that results in successful implantation [15, 16].

To attain the characteristics required for biomedical application, surface modifications such as sandblasting, acid etching, surface coating, alkali heat treatment, hydrothermal modification, plasma-spraying, ion implantation and pretreatment methods are employed. In spite of various available techniques, surface modification by chemical treatment has attracted the researcher due to its simple, cost-effective, bone-bonding ability and applicable to implants with complicated shapes. It has been reported that chemically treated titanium can induce the bone-like apatite formation on its surface. The reagents which are most frequently employed in the treatments are sodium hydroxide (NaOH) and hydrogen peroxide (H_2O_2) solutions. The sodium hydroxide treatment on titanium and its alloys produces porous sodium titanate gel layer, and the formed layer was found to induce the apatite formation and exhibited excellent corrosion resistance [17–25]. Karthega et al. [22] examined that the titania gel layer can also be produced using H_2O_2 treatment on the surface of pure titanium and it was found that 15 wt% H_2O_2 exhibits excellent in vitro bioactivity and higher corrosion resistance when compared with other concentrations. Wen et al. [26] evaluated the bioactivity of titanium alloy by two-step chemical treatment using the combination of acids ($HCl + H_2SO_4$) followed by alkali treatment. Aronsson et al. [27] studied the hydrogen thermal desorption from Cp-Ti subjected to acid etching ($HCl + H_2SO_4$ solution) and the results clearly indicating that Cp-Ti absorbs hydrogen during acid etching. Jonasova et al. [28] and Muller et al. [29] reported the influence of acid etching conditions on the microstructure of the Ti-13Nb-13Zr alloys as well as on the rate of HCA formation using SEM-EDX, FTIR and gravimetric analysis.

The objective of the present investigation is the surface modification of Ti-6Al-7Nb and Ti-5Al-2Nb-1Ta alloys using mixture of acids ($HCl + H_2SO_4$) followed by alkali and subsequent heat treatment to improve the bioactivity. The in vitro bioactivity of the specimens was evaluated by immersing in SBF solution. The surface and electrochemical characterization of surface-modified Ti-6Al-7Nb and Ti-5Al-2Nb-1Ta were evaluated for immediate and after 7 days of immersion in simulated body fluid (SBF) solution.

2 Materials and Methods

2.1 Specimen Preparation

Ti-6Al-7Nb (TIMET, UK) and Ti-5Al-2Nb-1Ta alloys (Kobe Steel Ltd., Japan) [17] with the size of dimension 1×1 cm^2 were used as the specimens, and its chemical compositions are presented in Table 1. The specimens were ground using abrasive SiC paper up to 1200# grade. Final polishing was done using alumina powder (0.5 μm in size) in order to produce a mirror finish surface followed by rinsing with distilled water and degreased with acetone. Further, the specimens were ultrasonicated in acetone for about 20 min. Finally, the specimens were washed in distilled water and dried in an oven.

2.2 Surface Treatment

The specimens were chemically etched with the mixture of acids ($HCl + H_2SO_4$) in the ratio (40 + 20) wt% maintained at room temperature (27 °C) for about 30 min. The acid-etched specimens were ultrasonically cleaned for 15 min in distilled water, dried and soaked in 10 M NaOH aqueous solution at 60 °C for 24 h. The specimens were then washed with distilled water and dried at 40 °C and subsequently heated at temperature of 600 °C with a rate of 5 °C/min for 1 h. Finally, the specimens were ultrasonically cleaned to remove the loosely attached particles over the surface.

2.3 Surface Characterization

X-ray diffraction patterns were recorded with Bruker D8 diffractometer using Cu-Kα radiation at a scan rate of (2θ) 0.02° min. The scanning range was from 20° to 50°. The surface morphology of the specimens was examined using SEM on a Hitachi model S-3400 coupled with EDAX. FTIR characterization was carried out in the range 400–4000 cm^{-1} on a Perkin-Elmer using the KBr technique.

2.4 Electrochemical Characterization

Electrochemical experiments were performed for all the specimens using a conventional three-electrode cell with potentiostat model (PGSTAT 12, AUTOLAB, the Netherlands B.V), which was controlled by a personal computer. A saturated Ag/AgCl electrode served as a reference electrode, platinum sheet acted as a counter

Table 1 Chemical compositions of Ti-6Al-7Nb and Ti-5Al-2Nb-1Ta alloys in (wt%)

Alloys	Al	V	Nb	O	C	N	H	Ni	Fe	Ta	Si	Ti
Ti-6Al-7Nb	5.85	0.01	6.95	0.17	0.001	0.01	0.003	0.01	0.20	0.05	0.63	Bal.
Ti-5Al-2Nb-1Ta	5.90	–	1.98	0.17	0.05	0.004	0.001	–	0.21	0.95	–	Bal.

electrode and the test specimens (Ti-6Al-7Nb and Ti-5Al-2Nb-1Ta alloys) as the working electrode with the exposed area of 1 cm^2. The SBF solution was used as the electrolyte, and the preparation of SBF and the in vitro experiments were performed using the procedure mentioned elsewhere [30].

Electrochemical impedance spectroscopic measurements were taken with a frequency ranging from 10^{-2} to 10^4 Hz using an electrochemical system frequency response analyser (FRA). The amplitude of the superimposed a.c. signal was 10 mV peak-to-peak voltages. The data obtained in terms of impedance spectra (Bode plots) were interpreted and fitted using a nonlinear least square (NLLS) method developed by Boukamp. Potentiodynamic polarization studies were carried out in the range of −1 to 2 V at a scan rate of 0.001 V/s using dedicated software. In order to obtain reliable results, polarization experiments were triplicated in SBF solution.

2.5 Mechanical Characterization

The micro-hardness measurements were taken using the micro-Vickers hardness tester (Wolpert group) to find out the strength of Ti-6Al-7Nb and Ti-5Al-2Nb-1Ta (three specimens of each). Hardness value is determined by the ratio of load and depth of the indentation with an indenter. The loads were applied at three different weights (10, 20 and 50 g), and the retention time was about 20 s.

3 Results and Discussion

3.1 Surface Characterization

The SEM micrographs of Ti-6Al-7Nb and Ti-5Al-2Nb-1Ta alloys are shown in Fig. 1. The UT (untreated) Ti-6Al-7Nb alloy revealed a dense and relatively smooth surface texture along with the unidirectional groove formation during the mechanical polish with no distinctive topographic features. After etching the surface using mixture of acids, it can be seen that a non-homogenous surface with ridges was formed over the surface. It clearly reveals that the Ti-6Al-7Nb alloy containing β phase has very low solubility compared to α phase and remains unattacked on the surface, forming very sharp ridges. The SEM micrograph of acid etched followed by alkali and heat-treated (AAHT) Ti-6Al-7Nb alloy showed a cracked and densified morphological surface. The cracked morphology could be due to the dehydration process that takes place during the heat treatment and leads to the formation of thick oxide layer. Further, the microporous reticulate structure formed during the AT (acid treatment) became finer. The UT Ti-5Al-2Nb-1Ta alloy showed smooth surface with unidirectional grooves formed during mechanical polish. After the acid treatment, both α and β grains exhibited a bridge-like structure of micro-pits with a sponge-like texture over the metal surface. Generally, α + β titanium alloys contain β-phase grains as an interstitial element surrounded by α-phase grains. During the acid etching, the β-phase grains dissolve and observed as white coloured bridges over the surface which can be attributed to the higher dissolution rate of β-phase grains compared to α-phase grains. The AAHT Ti-5Al-2Nb-1Ta alloy exhibited a cracked morphology which is similar to that of the AAHT Ti-6Al-7Nb alloy [27].

3.2 In Vitro Characterization

3.2.1 XRD Analysis

The XRD patterns for UT and AAHT Ti-6Al-7Nb alloy after 7 days of immersion in SBF solution are shown in Fig. 2a. The UT Ti-6Al-7Nb alloy showed the intense diffraction peaks at 2θ values of 26° and 31.5° corresponding to the planes of (002) and (211), and the AAHT Ti-6Al-7Nb alloy shows the intense diffraction peaks at 2θ values of 26°, 28.2°, 38.6°, 46° and 48.8° corresponding to the planes of (002), (210), (002), (111) and (312). These characteristic peaks represent the formation of crystalline apatite layer over the surface. The intensity of the diffraction peaks of AAHT Ti-6Al-7Nb alloy was high, which revealed the adsorption of Ca and P ions over the densified porous film. Li et al. also reported that the calcium phosphates as hydroxyapatite on oxidized and alkali-treated Ti-29Nb-13Ta-4.6Zr surface had been soaked in SBF solution [30].

The XRD patterns for UT and AAHT Ti-5Al-2Nb-1Ta alloy after 7 days of immersion in SBF solution are shown in Fig. 2b. The UT Ti-5Al-2Nb-1Ta alloy shows the intense diffraction peaks at 2θ values of 26.8° and 32° corresponding to the planes of (002) and (211) which indicated the apatite formation over the surface. The AAHT Ti-5Al-2Nb-1Ta alloy shows the intense sharp diffraction peaks at 2θ values of 26.8° and 49.2° corresponding to the planes of (002) and (222). These

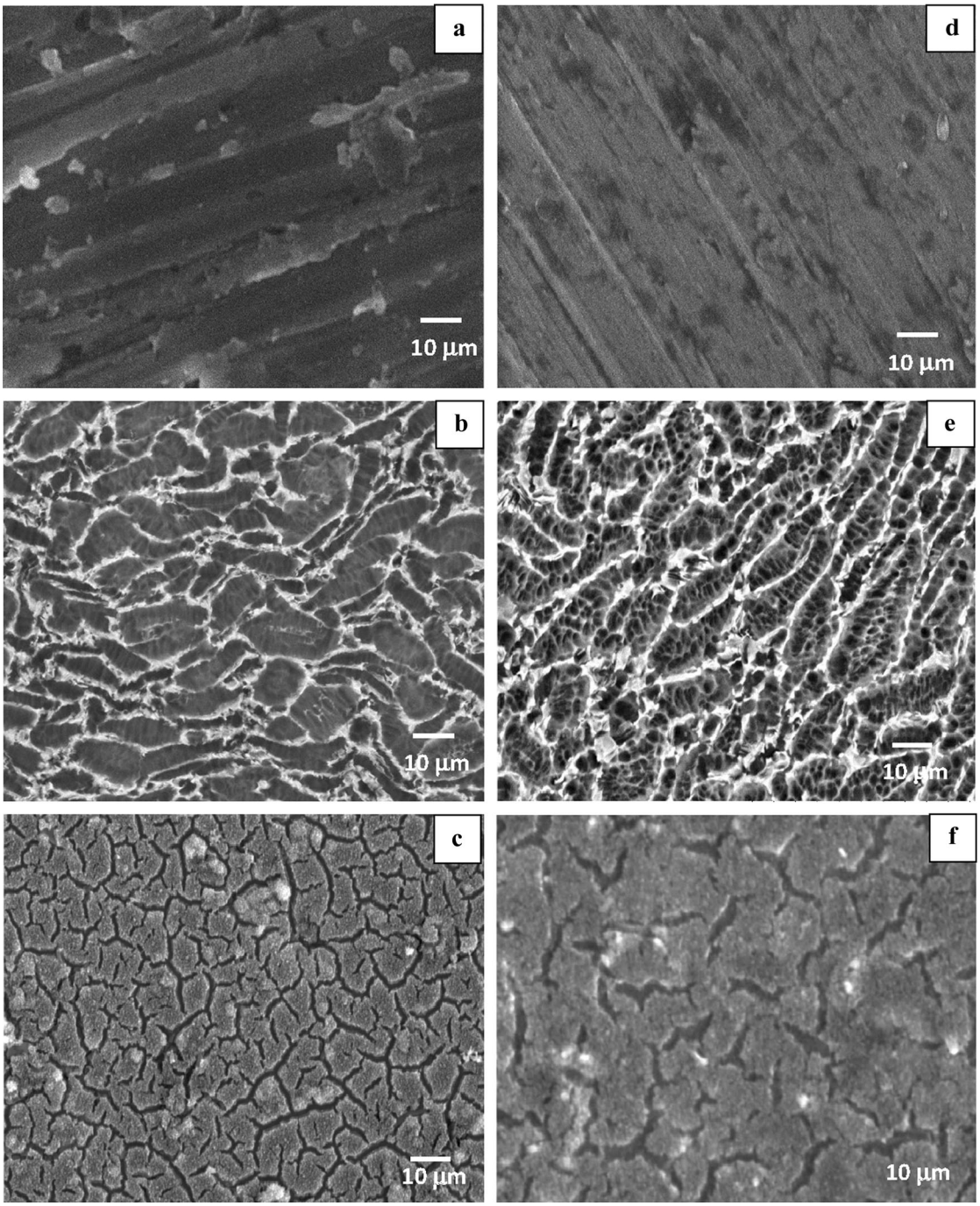

Fig. 1 SEM micrographs of Ti-6Al-7Nb and Ti-5Al-2Nb-1Ta alloys **a** UT, **b** AT, **c** AAHT, **d** UT, **e** AT and **f** AAHT

characteristic peaks represent the formation of crystalline apatite. However, the intensity of the diffraction peaks of AAHT Ti-5Al-2Nb-1Ta alloy becomes predominant due to the crystalline anatase phase over the specimens.

The average crystallite sizes of surface-modified Ti-6Al-7Nb and Ti-5Al-2Nb-1Ta alloys have been calculated using Scherer's equation [31]:

$$D_{hkl} = k\lambda/[B\cos\theta] \quad (1)$$

where B is the full width half maximum (FWHM) of the peaks of the pure diffraction profile in radians, k is a constant (shape factor 0.89), λ is the wavelength of the X-rays (0.1540 nm), θ is the diffraction angle and D_{hkl} is the average diameter of the crystallite. From the estimated

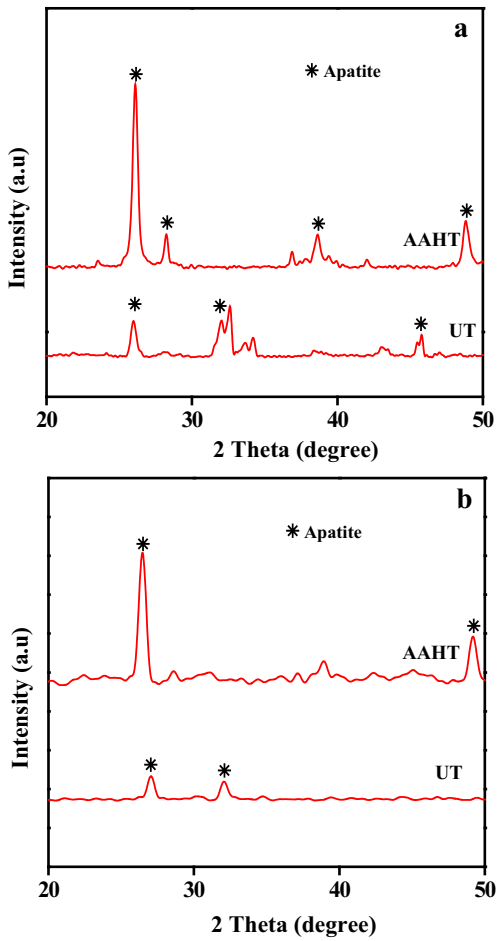

Fig. 2 XRD patterns of **a** Ti-6Al-7Nb and **b** Ti-5Al-2Nb-1Ta alloys after 7 days of immersion in SBF solution

data, the calculated average crystallite sizes were found in the range of 30–50 nm, respectively, for all the specimens.

3.2.2 FTIR Analysis

The FTIR spectrum of the UT, AAHT Ti-6Al-7Nb and Ti-5Al-2Nb-1Ta alloys immersed in SBF solution for 7 days is shown in Fig. 3. A broad absorption band at about 3446 cm^{-1} and the bending modes at 1648 and 1632 cm^{-1} revealed the O–H stretching and bending vibrations of adsorbed H_2O. The presence of PO_4^{3-} group is also ascertained from the peaks at 1038 cm^{-1}. The presence of CO_3^{2-} peak was assigned at 1458 and 1400 cm^{-1}. The triply (ν_4) and doubly (ν_2) degenerated bending modes of phosphates O–P–O bonds were found at 601 and 547 cm^{-1} [32, 33]. The peaks corresponding to the phosphate and carbonate functional groups immersed for 7 days confirmed the formation of apatite layer and also the grown layer which is essentially the carbonate incorporated apatite.

3.2.3 SEM-EDAX Studies

The SEM-EDAX micrographs of UT, AAHT Ti-6Al-7Nb and Ti-5Al-2Nb-1Ta alloys immersed in SBF solution for 7 days are depicted in Figs. 4 and 5. After soaking in SBF solution, the morphology and the composition of the UT, AAHT Ti-6Al-7Nb and Ti-5Al-2Nb-1Ta specimens exhibited significant variations, confirming the materials ability to interact with the ions present in the SBF solution. It could be observed that only a few white particles formed randomly over the surface for UT Ti-6Al-7Nb and Ti-5Al-2Nb-1Ta specimens, whereas in the case of AAHT Ti-6Al-7Nb alloy an isolated globular-shaped apatite-like particles were found over the entire surface of the specimen, which could be due to the prolonged interaction of calcium and phosphate ions adsorbed on the surface of the modified specimens. On the other hand, the AAHT Ti-5Al-2Nb-1Ta alloy revealed a cluster of spherical apatite-like particles randomly on the porous sodium titanate layer, formed after the heat treatment which may be due to the low adsorption of Ca and P ions in the SBF solution [34]. The Ca/P ratio of all the specimens was found to be 1.67 from the EDAX analysis.

3.2.4 Mechanism

Treated titanium forms bone-like apatite layer on their surfaces when immersed in SBF solution. These apatite layers are formed over the surface through different mechanisms depending on the type of pretreatment adopted before immersion in SBF solution.

During acid (H_2SO_4 + HCl) etching, the passive oxide film degradates as follows

$$2TiO_2 + 2(H_2SO_4 + 2HCl) \rightarrow Ti(SO_4)_2 + TiCl_4 + 4H_2O \quad (2)$$

Simultaneously, titanium reacts with HCl to form $TiCl_3$ and H_2:

$$2Ti + 2(H_2SO_4 + 3HCl) \rightarrow Ti(SO_4)_2 + 2TiCl_3 + 5H_2 \quad (3)$$

TiH_2 was can be formed by

$$Ti + H_2 \rightarrow TiH_2 \quad (4)$$

On the TiH_2 intermediate layer, a new oxide layer can form in contact with air moisture. It can be supposed that the titanium oxide layer is thinner than the initial one because it was not exposed to high temperature. Upon exposure of acid-etched titanium in NaOH, the passive oxide layer dissolves to form amorphous titania layer containing Na^+ ions.

$$TiO_2 + NaOH \rightarrow HTiO_3^- + Na^+ \quad (5)$$

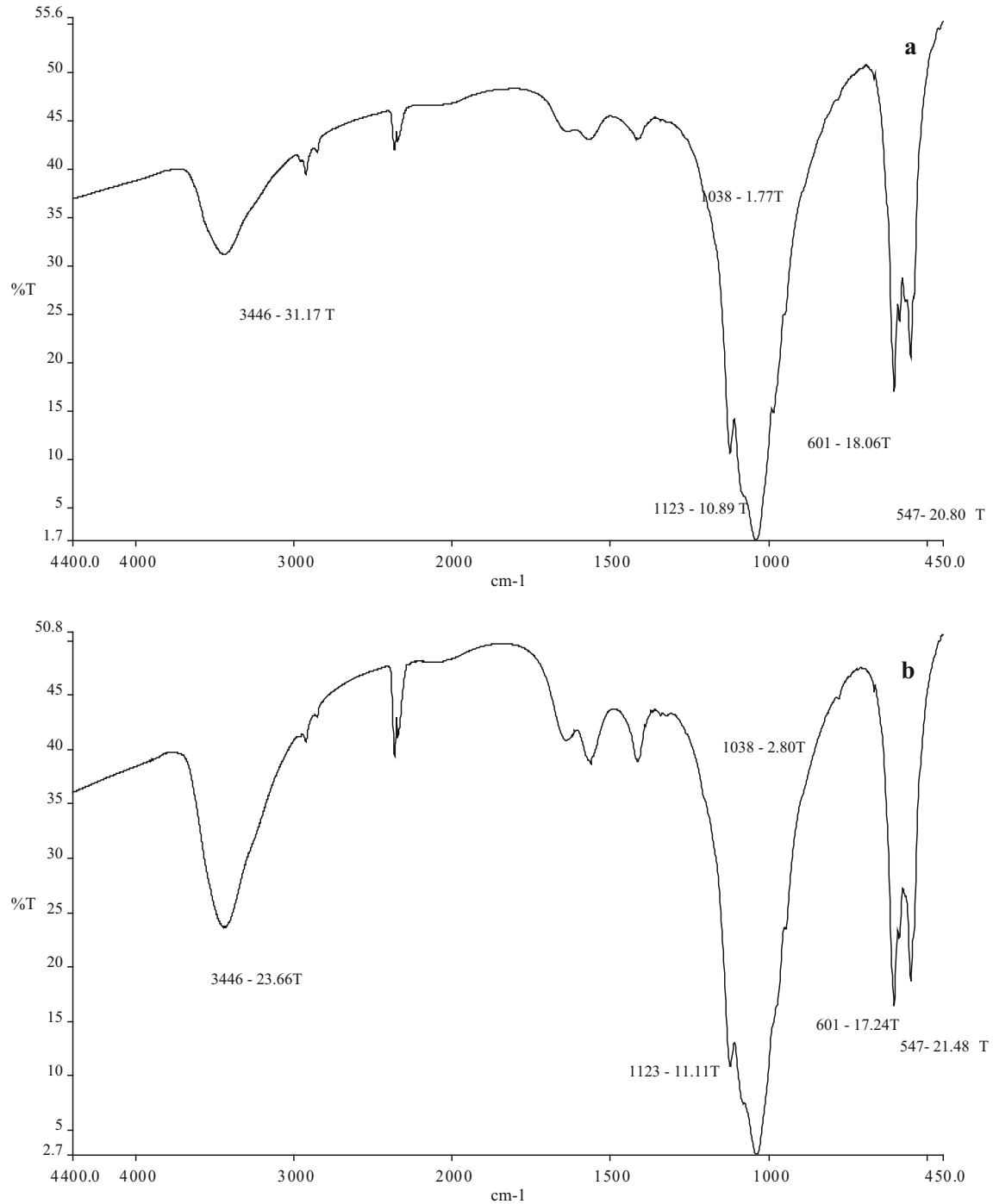

Fig. 3 FTIR spectrum of **a** Ti-6Al-7Nb and **b** Ti-5Al-2Nb-1Ta alloys after 7 days of immersion in SBF solution

When the AAHT specimen is soaked in SBF solution, Na^+ ions from the amorphous layer will be exchanged by H_3O^+ ions from the surrounding fluid resulting in Ti–OH layer formation.

$$[TiO_2]\text{solid} + 2H_2O \Leftrightarrow [TiO_2 \cdot OH]^-_{(aq)} + H_3O^+ \quad (6)$$

Simultaneously, with increasing pH the apatite nucleation is accelerated by increasing the super saturation of the solution with respect to apatite. Calcium ions are incorporated in the hydrated Ti–OH layer. The positively charged Ca^{2+} may act as nucleation sites for HCA by attaching to negatively charged $(PO_4)^{3-}$ and $(CO_3)^{2-}$ to form Ca–P-enriched surface layer which crystallizes to bone-like apatite (HCA) [26, 27].

$$10Ca^{2+} + 6PO_4^{3-} + 2OH^- \leftrightarrow Ca_{10}(PO_4)_6(OH)_2 \quad (7)$$

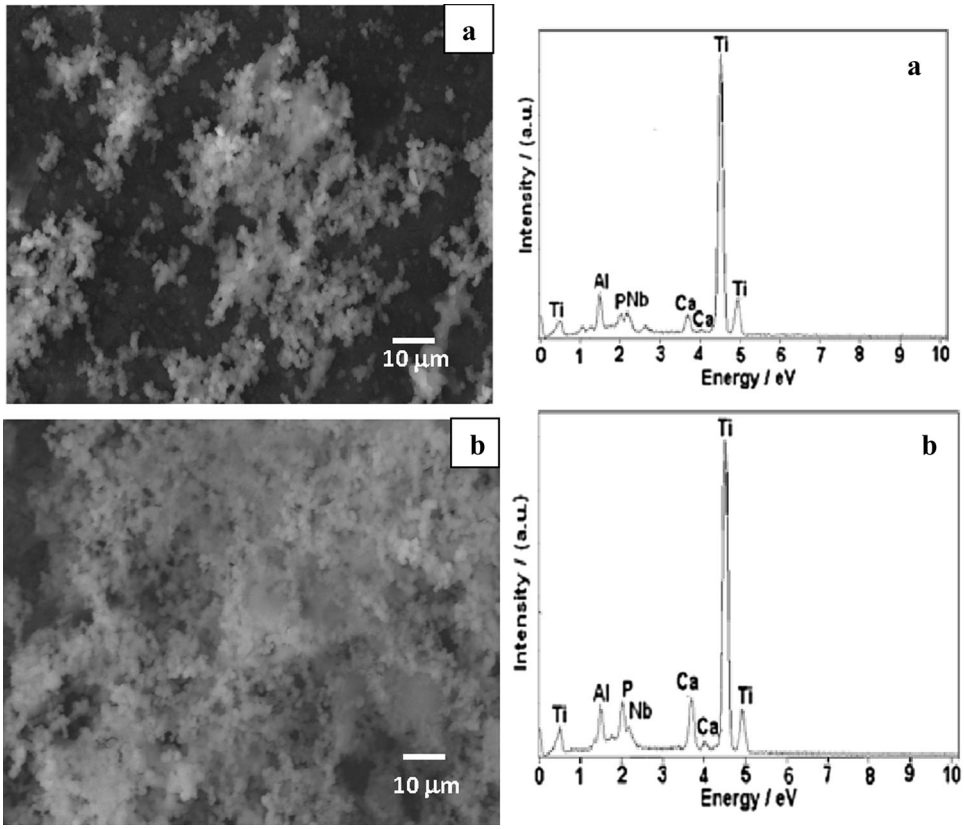

Fig. 4 SEM-EDAX micrographs of Ti-6Al-7Nb alloy **a** UT and **b** AAHT after 7 days of immersion in SBF solution

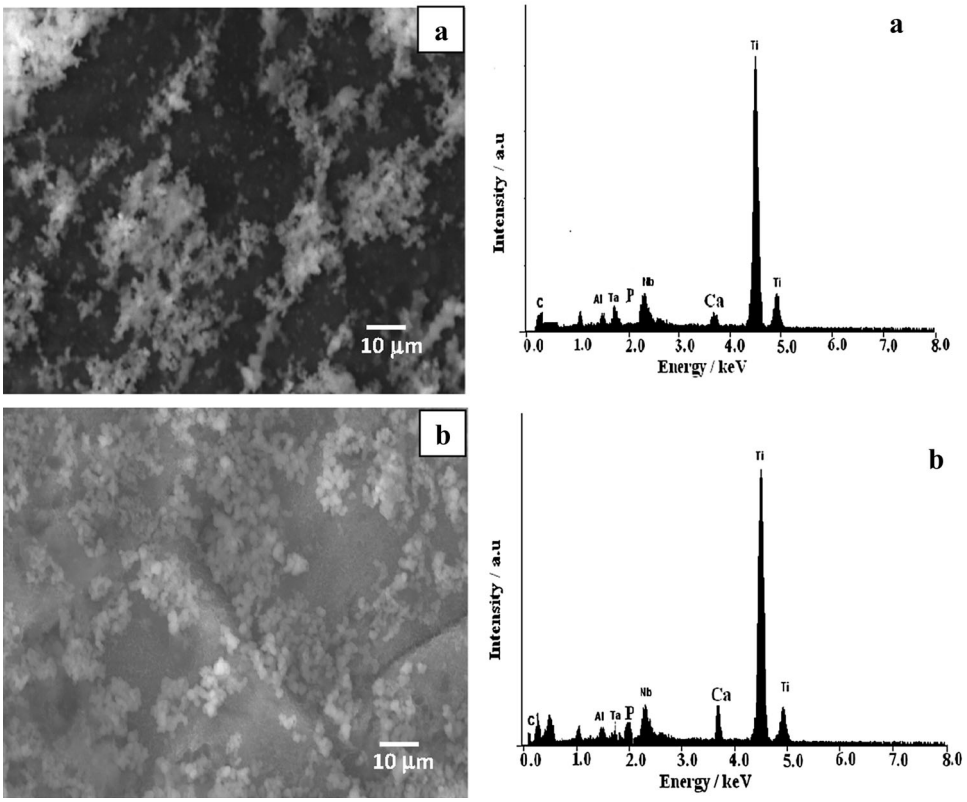

Fig. 5 SEM-EDAX micrographs of Ti-5Al-2Nb-1Ta alloy **a** UT and **b** AAHT after 7 days of immersion in SBF solution

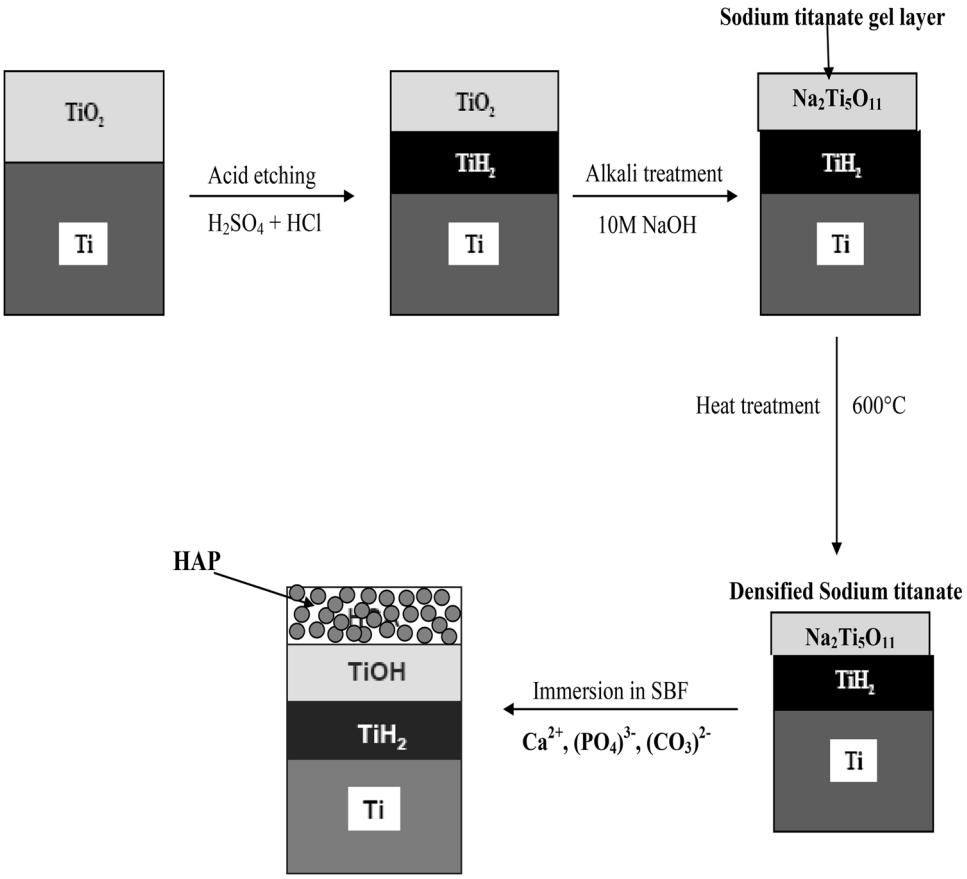

Schematic representation of surface modification of titanium followed by the apatite growth

3.3 Electrochemical Characterization

The electrochemical characterization was performed in order to evaluate the protective effectiveness of the surface layer formed on the Ti-6Al-7Nb and Ti-5Al-2Nb-1Ta alloys during acid etching followed by alkali heat treatment. The surface-modified specimens were then subjected to potentiodynamic polarization and electrochemical impedance spectroscopy.

3.3.1 Potentiodynamic Polarization Results

Potentiodynamic polarization plots obtained for UT, AAHT Ti-6Al-7Nb and UT, AAHT Ti-5Al-2Nb-1Ta on immersion in SBF solution are presented in Figs. 6 and 7. The UT Ti-6Al-7Nb alloy (Fig. 6a) exhibits a stable passive film extending over a wide range of potentials with constant current density. However, AAHT Ti-6Al-7Nb alloy shows a stable current density remained till 1.5 V, and there is a slight increase in the anodic current density beyond 1.5 V which could be mainly due to the breakdown of the titanate layer. It can be observed that the corrosion potential values for UT and AAHT Ti-6Al-7Nb were found to be -0.49 V and -0.38 V, respectively. The UT Ti-5Al-2Nb-1Ta (Fig. 7a) shows a stable passive film at a potential region of 0.1–1 V. At this region, the current density remains almost same, which indicates the thickening of the anodic surface film. The AAHT Ti-5Al-2Nb-1Ta alloy (Fig. 7a) shows a stable current density which remained same till 1 V and beyond 1 V, and there is a slight increase in the anodic current density, which is due to the breakdown of the porous titanate layer in SBF solution [34]. The corrosion potential values for UT and AAHT Ti-5Al-2Nb-1Ta were found to be −0.30 and −0.19 V, respectively.

To study the effect of immersion time on corrosion behaviour of Ti-6Al-7Nb and Ti-5Al-2Nb-1Ta alloys in SBF solution, potentiodynamic polarization measurements were taken after 7 days. AAHT Ti-6Al-7Nb exhibited a significant shift of potential in the nobler direction and a steady decrease in the corrosion current density with one order of magnitude when compared with AAHT Ti-5Al-2Nb-1Ta. From this, we can infer that due to the prolonged interaction of Ca and P ions from the SBF solution forms a porous film over the AAHT Ti-6Al-7Nb surfaces which enhance the corrosion resistance.

Tamilselvi et al. [18] have examined that the passive current density was almost constant for the alkali heat-

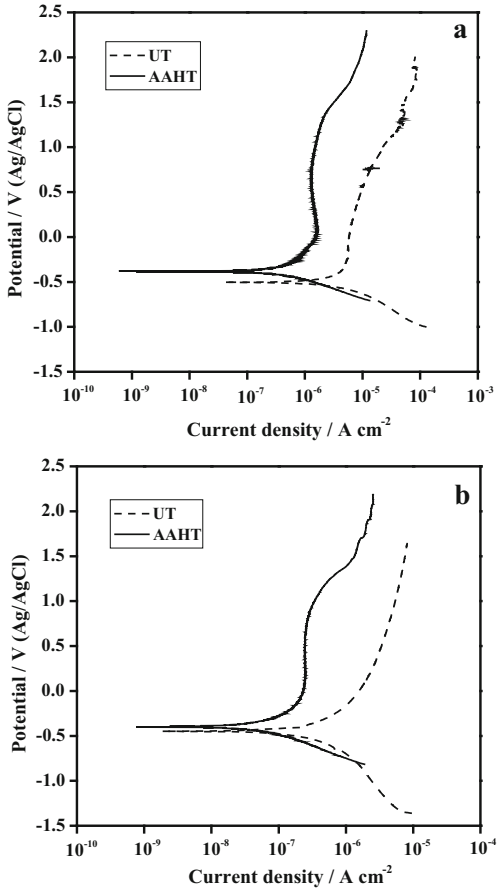

Fig. 6 Potentiodynamic polarization curves of Ti-6Al-7Nb alloy **a** immediate and **b** 7 days

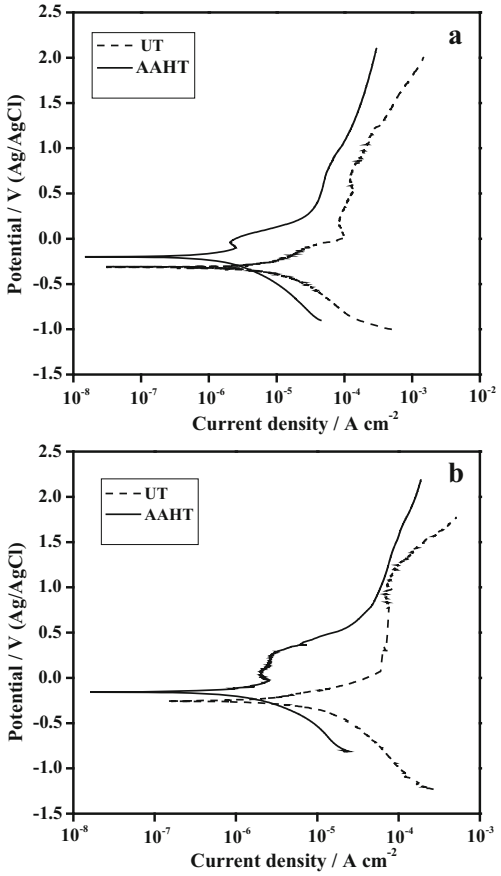

Fig. 7 Potentiodynamic polarization curves of Ti-5Al-2Nb-1Ta alloy **a** immediate and **b** 7 days

treated Ti-6Al-7Nb alloys after 7 days of immersion in SBF solution. The results revealed that there is a decrease in the current density with increase in the immersion time which can be attributed to the densification of film during the alkali heat treatment and also a prolonged interaction of calcium and phosphate ions present in the Hanks solution forms an apatite layer which improves corrosion resistance. Assis et al. [35] have also examined the similar observations on Ti-6Al-7Nb alloy immersed in SBF medium.

3.3.2 Electrochemical Impedance Spectroscopic Results

Electrochemical impedance response of UT Ti-6Al-7Nb alloy on immediate and after 7 days of immersion in SBF solution is presented in Fig. 8a. It can be observed that the UT Ti-6Al-7Nb alloy shows a near-capacitive response which is the indicative of a typical thin single passive oxide film present on the metal surface which is highly insulative and protective against aggressive ion ingression. However, after 7 days of immersion in SBF solution, the UT Ti-6Al-7Nb alloy shows a significant shift in the phase angle on the whole of the frequency region [34]. This behaviour confirms the formation of a new layer (apatite as confirmed from XRD and SEM-EDAX).

Electrochemical impedance response of AAHT Ti-6Al-7Nb alloy on immediate and after 7 days of immersion in SBF solution is presented in Fig. 8b. The AAHT Ti-6Al-7Nb alloy exhibited two well-defined distinct humps in the higher- and lower-frequency regions which indicated the presence of duplex layers, with inner barrier layer and outer porous densified gel layer due to the heat treatment over the surface of Ti-6Al-7Nb alloy. However, after 7 days of immersion in SBF solution, spectra exhibited triplex layers with inner barrier layer, outer porous layer and formation of a new layer. The formation of a new layer is the characteristics of a shift in the phase angle at the low-frequency region. The shift in the phase angle can be attributed to the growth of apatite over AAHT Ti-6Al-7Nb alloy. The interaction of solutions is generally identified by a phase shift at the higher-frequency region which can be attributed to a physical change in the porous layer due to the interaction of the solution ions present in the solution [36].

Electrochemical impedance response of UT Ti-5Al-2Nb-1Ta alloy on immediate and after 7 days of immersion in SBF solution is presented in Fig. 9a. UT Ti-5Al-2Nb-1Ta alloy

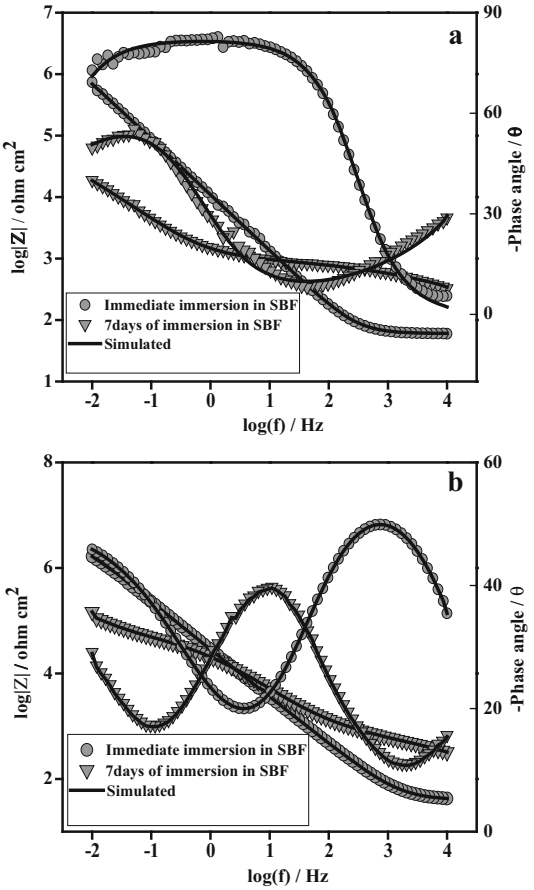

Fig. 8 Bode-phase angle and Bode-impedance plot of **a** UT Ti-6Al-7Nb alloy and **b** AAHT Ti-6Al-7Nb alloy on immersion in SBF solution

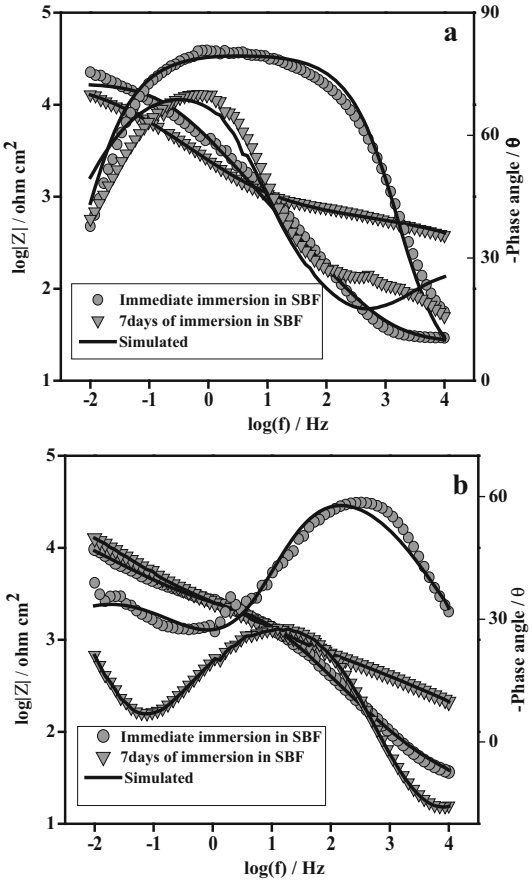

Fig. 9 Bode-phase angle and Bode-impedance plot of **a** UT Ti-5Al-2Nb-1Ta alloy and **b** AAHT Ti-5Al-2Nb-1Ta alloy on immersion in SBF solution

exhibited similar type of observations of UT Ti-6Al-7Nb alloy. After 7 days of immersion in SBF solution, the spectra exhibited a duplex layer of inner barrier and outer porous layer, respectively. Electrochemical impedance response of AAHT Ti-5Al-2Nb-1Ta alloy on immediate and after 7 days of immersion in SBF solution is presented in Fig. 9b. AAHT Ti-5Al-2Nb-1Ta alloy shows a similar behaviour to that of AAHT Ti-6Al-7Nb alloy. However, after the seventh day of immersion, the spectra exhibited only duplex layers with inner barrier layer and outer apatite layer [36].

From the impedance plots, it can be inferred that the solution resistance (R_s) is high for AAHT Ti-6Al-7Nb and Ti-5Al-2Nb-1Ta which indicated the adsorption of solution ions over the surface, creating a high solution resistance. This also suggests that repair of the defects in the barrier layer during the period of immersion might have occurred by the incorporation of mineral ions from the solution into the defects/pores or to the film thickening during immersion time [22].

Impedance values were derived from the plots and are presented in Tables 2 and 3. It can be observed that R_b values found to be increase with increase in immersion time, whereas R_p values decrease which indicate that the impedance response is dominated by the presence of barrier layer. The increase in R_b value indicates the increase in the passive film thickness. This suggests that there is a change in the passive film behaviour of Ti-6Al-7Nb and Ti-5Al-2Nb-1Ta due to the newly formed layer that accounts for the higher protection. This shows that the corrosion of Ti-6Al-7Nb and Ti-5Al-2Nb-1Ta is prohibited by non-porous inner layer and facilitated the growth of oxide layer [22]. It can be seen that R_a values for AAHT Ti-6Al-7Nb are found to be higher of 7194 KΩ cm^2 which represents the formation of an strong apatite layer after 7 days of immersion in SBF solution when compared with other specimens.

From the electrochemical studies, it can be concluded that AAHT Ti-6Al-7Nb exhibited higher corrosion potential and lower current density from the results obtained from polarization and impedance measurements. This indicates that the thickness of CaP layer formed is higher and AAHT Ti-6Al-7Nb exhibited excellent in vitro bioactivity.

Table 2 Impedance parameters of Ti-6Al-7Nb and Ti-5Al-2Nb-1Ta alloys obtained by fitting R_s (R_bQ_b) and R_s (R_pQ_p) (R_bQ_b) model for immediate immersion in SBF solution

Specimens	R_s/Ω cm^2	R_p/KΩ cm^2	Q_p/μF cm^{-2}	n	R_b/KΩ cm^2	Q_b/μF cm^{-2}	n
UT Ti-6Al-7Nb	44	–	–	–	1803	0.32	0.88
AAHT Ti-6Al-7Nb	109	6232	1.75	0.82	1642	9.53	0.90
UT Ti-5Al-2Nb-1Ta	48	–	–	–	1483	3.95	0.85
AAHT Ti-5Al-2Nb-1Ta	124	4005	4.87	0.82	1556	7.80	0.89

Table 3 Impedance parameters of Ti-6Al-7Nb and Ti-5Al-2Nb-1Ta alloys obtained by fitting R_s (R_aQ_a) (R_pQ_p) (R_bQ_b) and R_s (R_aQ_a) (R_bQ_b) model after 7 days of immersion in SBF solution

Specimens	R_s/Ω cm^2	R_a/KΩ cm^2	Q_a/μF cm^{-2}	n	R_p/KΩ cm^2	Q_p/μF cm^{-2}	n	R_b/KΩ cm^2	Q_b/μF cm^{-2}	n
UT Ti-6Al-7Nb	49	4923	0.89	–	–	–	–	2544	2.46	0.86
AAHT Ti-6Al-7Nb	114	7194	0.45	0.81	5138	3.53	0.81	2645	7.64	0.86
UT Ti-5Al-2Nb-1Ta	52	4121	3.78	0.84	–	–	–	2575	4.67	0.81
AAHT Ti-5Al-2Nb-1Ta	138	4112	2.73	0.79	–	–	–	2324	5.96	0.87

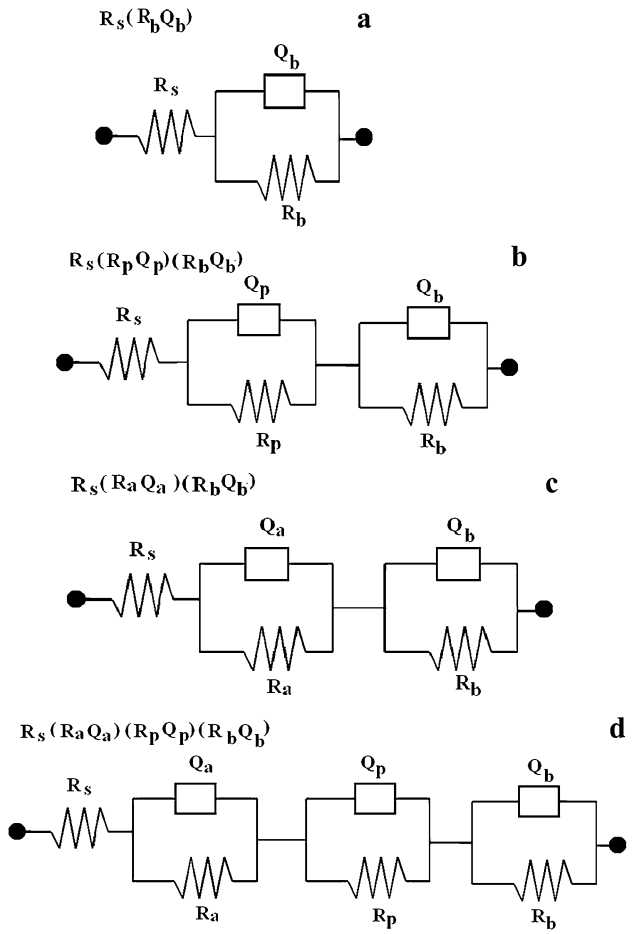

Fig. 10 Equivalent circuit diagrams of Ti-6Al-7Nb and Ti-5Al-2Nb-1Ta alloys **a**, **b** immediate and **c**, **d** 7 days

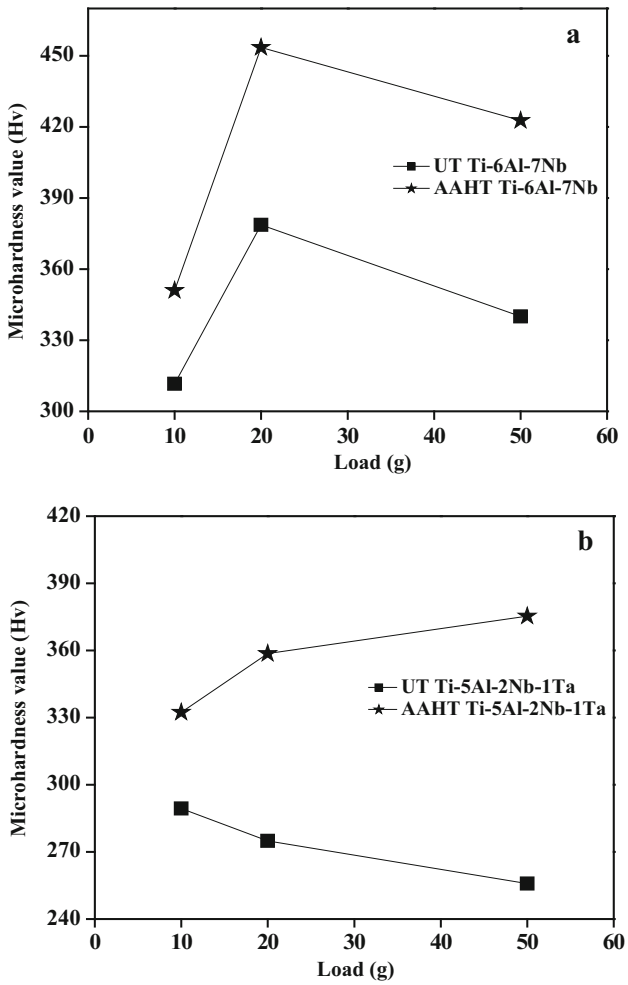

Fig. 11 Micro-hardness values of **a** Ti-6Al-7Nb and **b** Ti-5Al-2Nb-1Ta alloys

Table 4 Vickers micro-hardness measurements of (a) Ti-6Al-7Nb and (b) Ti-5Al-2Nb-1Ta alloys

Material used	Condition	Load (g)	Vicker hardness value (VHN)	Average hardness values
Ti-6Al-7Nb	UT	10	311.6	343.4
		25	378.7	
		50	340.0	
	AAHT	10	351.0	409.2
		25	453.6	
		50	422.7	
Ti-5Al-2Nb-1Ta	UT	10	289.4	273.3
		25	274.9	
		50	255.8	
	AAHT	10	332.4	355.4
		25	358.6	
		50	375.3	

The equivalent circuit proposed for the UT Ti-6Al-7Nb and Ti-5Al-2Nb-1Ta are R_s (R_bQ_b) is shown in Fig. 10a where R_s represents the solution resistance and R_b and Q_b represent the charge transfer resistance and double-layer capacitance of the barrier layer. This represents the presence of a single layer on the metal surface possessing resistance as well as capacitance. The obtained impedance spectra for AAHT Ti-6Al-7Nb and Ti-5Al-2Nb-1Ta alloys were fitted using $R_s(R_pQ_p)$ (R_bQ_b), where R_p and Q_p represent the resistance and capacitance of the porous layer and are characterized by two parallel combination of resistance and capacitance in series with the solution resistance (Fig. 10b). It indicated the formation of duplex layer, viz. inner barrier layer and outer porous layer. Similar type of circuit was proposed to simulate the data for titanium in SBF solution and can be considered as an equivalent circuit representation of a two layer model of the oxide film, consisting of an inner barrier and outer porous layer [22]. The equivalent circuit model proposed for UT Ti-6Al-7Nb and Ti-5Al-2Nb-1Ta alloys and AAHT Ti-5Al-2Nb-1Ta alloy after 7 days of immersion in SBF solution is presented in Fig. 10c. The circuit model can be represented as R_s (R_aQ_a) (R_bQ_b), where R_a and Q_a represent the resistance and capacitance of the apatite layer shown in Fig. 10d. The model which is used to fit the spectra obtained for AAHT Ti-6Al-7Nb is represented as $R_s(R_aQ_a)$ (R_pQ_p) (R_bQ_b) which exhibited the presence of triplex layer, indicated the formation of a new layer which may be due to the adsorption of calcium and phosphate ions over the porous layer.

3.4 Mechanical Characterization

To examine the changes in hardness, the micro-hardness measurements were taken for UT, AAHT Ti-6Al-7Nb and Ti-5Al-2Nb-1Ta specimens and the micro-hardness data of UT and AAHT specimens at various applied loads of 10, 20 and 50 gms are presented in Fig. 11 (a-b). It can be seen that a considerable increase in the hardness values for the AAHT Ti-6Al-7Nb alloy compared with the other specimens as shown in Table 4. This could be due to densification of porous titanate layer formed over the metal surface during the acid etching with alkali and heat treatment [35].

4 Conclusions

Ti-6Al-7Nb and Ti-5Al-2Nb-1Ta alloys were subjected to surface modification by two-step chemical treatments and subsequent heat treatment to enhance the bone-bonding ability of the implants. Surface characterization revealed the porous anatase gel layer over the specimens. In vitro characterization revealed that the treatment of Ti-6Al-7Nb and Ti-5Al-2Nb-1Ta alloys with mixture of acids was prospectively found to have better bone-bonding ability and the growth of apatite layer was also confirmed by FTIR and XRD analysis. The potentiodynamic polarization studies revealed that the AAHT specimens after 7 days of immersion in SBF solution exhibited lower current density compared to the UT specimens. The electrochemical impedance spectroscopic results revealed the appearance of duplex layer for the immediate immersion and exhibited triplex layer after 7 days of immersion in SBF solution for the AAHT Ti-6Al-7Nb. The AAHT Ti-5Al-2Nb-1Ta revealed a duplex layer for immediate and after 7 days of immersion in SBF solution.

Hence, the AAHT Ti-6Al-7Nb alloy enhances the biocompatibility with higher hardness value and induces the apatite forming ability within a short period of time and also exhibited improved corrosion resistance compared with the AAHT Ti-5Al-2Nb-1Ta which is widely used as orthopaedic implants.

Acknowledgement The authors acknowledge the Council of Scientific and Industrial Research (CSIR), New Delhi, for their financial support.

References

1. Sitting C, Textor M, Spencer ND, Wieland M, Vallotton PH (1999) Surface Characterization. J Mater Sci Mater Med 10:35–46
2. Niinomi M, Kuroda D, Fukunaga K, Morinaga M, Kato Y, Yashiro T, Suzuki A (1999) Corrosion wear fracture of new beta type biomedical Ti alloys. Mater Sci Eng, A 263:193–199
3. Okazaki Y (2002) Effect of friction on anodic polarization properties of metallic biomaterials. Biomaterials 23:2071–2077
4. Khan MA, Williams RL, Williams DF (1999) Conjoint corrosion and wear in Ti alloys. Biomaterials 20:765–772
5. Khan MA, Williams RL, Williams DF (1996) In-vitro corrosion and wear in Ti alloys in biological environments. Biomaterials 17:2117–2126
6. Khan MA, Williams RL, Williams DF (1999) The corrosion behavior of Ti-6Al-4V, Ti-6Al-7Nb and Ti-13Nb-13Zr in protein solutions. Biomaterials 20:631–637
7. Niinomi M (1998) Mechanical properties of biomedical Ti alloys. Mater Sci Eng, A 243:231–236
8. Wang K (1996) The use of Ti for medical applications in the USA. Mater Sci Eng A 213:134–137
9. Semlitsch MF, Weber H, Streicher RM, Schon R (1992) Joint replacement components made of hot-forged and surface-treated Ti-6Al-7Nb alloy. Biomaterials 13:781–788
10. Rack HJ, Qazi JI (2006) Titanium alloys for biomedical applications. Mat Sci Eng C 26(8):1269–1277
11. Manivasagam G, Dhinasekaran D, Rajamanickam A (2010) Biomedical implants: corrosion and its prevention—a review. Recent Patents Corros Sci 2:40–54
12. Jaganathan SK, Supriyanto E, Murugesan S, Balaji A, Asokan MK (2014) Biomaterials in cardiovascular research: applications and clinical implications. Bio Med Res Int 2014:459465. doi:10.1155/2014/459465
13. Jaganathan SK, Balaji A, Vellayappan MV, Subramanian P, John AA, Asokan MK, Supriyanto E (2015) Review: radiation-induced surface modification of polymers for biomaterial application. J Mat Sci 50:2007–2018
14. Liu X, Chub PK, Ding C (2004) Surface modification of titanium, titanium alloys, and related materials for biomedical applications. Mat Sci Eng R47:49–121
15. Kulkarni M, Mazare A, Schmuki P, Iglič A (2014) Biomaterial surface modification of titanium and titanium alloys for medical applications. In: Seifalian A (ed) Nanomedicine. One Central Press, Manchester, pp 111–113
16. Wong M, Eulenberger J, Schenk R, Hunziker E (1995) Effect of surface topology on the osseointegration of implant materials in trabecular bone. J Biomed Mater Res 29:1567–1575
17. Tamilselvi S, Balaji-Raghavendran H, Srinivasan P, Rajendran N (2009) In vitro and In vivo Studies of alkali and alkali heat treated Ti-6Al-7Nb and Ti-5Al-2Nb-1Ta alloys for orthopaedic implants. J Biomed Mater Res Part A 90:380–386
18. Tamilselvi S, Raman V, Rajendran N (2009) Corrosion behavior of titanium alloys in Hanks solution. Trans Mater Res Soc Japan 34:579–583
19. Tamilselvi S, Raman V, Rajendran N (2010) Surface modification of titanium by chemical and thermal methods—electrochemical impedance spectroscopic studies. Corros Eng Sci Technol 46:585–591
20. Raman V, Tamilselvi S, Rajendran N (2007) Electrochemical impedance spectroscopic characterisation of titanium during alkali treatment and apatite growth in simulated body fluid. Electrochim Acta 52:7418–7424
21. Sasikumar Y, Karthega M, Rajendran N (2010) In vitro bioactivity of surface-modified β-Ti alloy for biomedical applications. J Mater Eng Perform 20:1271–1277
22. Karthega M, Nagarajan S, Rajendran N (2010) In vitro studies of hydrogen peroxide treated titanium for biomedical applications. Electrochim Acta 55:2201–2209
23. Indira K, Mudali UK, Nishimura T et al (2015) A review on TiO_2 nanotubes: influence of anodization parameters, formation mechanism, properties, corrosion behavior, and biomedical applications. J Bio Tribo Corros 1:28. doi:10.1007/s40735-015-0024-x
24. Indira K, Kamachi Mudali U, Rajendran N (2017) Development of self-assembled titania nanopore arrays for orthopedic applications. J Bio Tribo Corros 3:9. doi:10.1007/s40735-016-0068-6
25. Indira K, Mudali UK, Rajendran N (2014) In-vitro biocompatibility and corrosion resistance of strontium incorporated TiO_2 nanotube arrays for orthopaedic applications. J Biomater Appl 29:113–129
26. Wen HB, Wolke JG, Wijn JR, Liu Q, de Cui FZ, Groot K (1997) Fast precipitation of calcium phosphate layers on titanium induced by simple chemical treatments. Biomaterials 18:1471–1478
27. Aronsson BO, Hjörvarsson B, Frauchiger L, Taborelli M, Vallotton PH, Descounts P (2001) Hydrogen desorption from sand-blasted and acid-etched titanium surfaces after glow-discharge treatment. J Biomed Mater Res 54:20–29
28. Jonasova L, Muller FA, Helebrant A, Strnad J, Greil P (2004) Biomimetic apatite formation on chemically treated titanium. Biomaterials 25:1187–1194
29. Muller FA, Bottinob MC, Muller L, Henriquesd VAR, Lohbauere U, Bressianib AHA, Bressianib JC (2008) In vitro apatite formation on chemically treated (P/M) Ti–13Nb–13Zr. Dent Mater 24:50–56
30. Li SJ, Yang R, Niinomi M, Hao YL, Cui YY (2004) Formation and growth of calcium phosphate on the surface of oxidized Ti-29Nb-13Ta-4.6Zr Alloy. Biomaterials 25:2525–2532
31. Lindgren T, Muabora JH, Avendeno E, Jonsson J, Hoel A, Granquist CG, Lindquist SE (2003) Photo electrochemical and optical properties of nitrogen doped titanium dioxide films prepared by reactive DC magnetron sputtering. J Phys Chem B 107:5709–5716
32. Koutsopoulos S (2002) Synthesis and characterization of hydroxyapatite crystals: a review study on the analytical methods. J Biomed Mater Res 62:600–612
33. Liang F, Zhou L, Wang K (2003) Apatite formation on porous titanium by alkali and heat-treatment. Surf Coat Technol 165:133–139
34. Sasikumar Y, Rajendran N (2013) Influence of surface modification on the apatite formation and corrosion behavior of Ti and Ti-15Mo alloy for biomedical applications. Mater Chem Phys 138:114–123
35. Assis S, Wolynee S, Costa I (2006) Corrosion characterization of titanium alloys by electrochemical techniques. Electrochim Acta 51:1815–1819
36. Hodgson AWE, Mueller Y, Forster D, Virtanen S (2002) Electrochemical characterisation of passive films on Ti Alloys under simulated biological condition. Electrochim Acta 47:1913–1923